IAHR
AIRH

Journal of Hydraulic Research Vol. 00, No. 0 (2007), pp. 1–9

The effect of floodplain roughness on flow structures, bedforms and sediment transport rates in meandering channels with overbank flows: Part II

K. SHIONO, *Department of Civil and Building Engineering, Loughborough University, Loughborough, LE11 3TU, UK. E-mail: K.Shiono@lboro.ac.uk*

T. CHAN, *Atkins Water, Peterborough, UK. E-mail: TuckLeong.Chan@atkinsglobal.com*

J. SPOONER, *Riley Consultants Limited, Auckland, New Zealand. E-mail: jake@jakespooner.co.uk*

P. RAMESHWARAN, *Centre for Ecology and Hydrology, Crowmarsh Gifford, Wallingford, Oxfordshire, OX10 8BB, UK. E-mail: ponr@ceh.ac.uk*

J.H. CHANDLER, *Department of Civil and Building Engineering, Loughborough University, Loughborough, LE11 3TU, UK. E-mail: J.H.Chandler@lboro.ac.uk*

ABSTRACT

A series of experiments were conducted to understand the behaviour of flow resistance and sediment transport rate within compound meandering channel whilst changing floodplain roughness. The detailed flow structures with bedforms were reported in Part I of this paper. This second sister paper concentrates on the behaviour of bedforms, sediment transport rate and flow resistance during flood conditions. The bedforms along the meandering channel with various overbank flows are presented and interesting bed features observed. The changing sediment transport rates with various water depths are also shown and the sediment transport rate first decreases and then increases during flood. The initiation of this increase appears closely related to the ratio of the floodplain velocity to the main channel velocity in this configuration. The Manning n values in the meandering are established using both the sediment transport data and the velocity data from Part I. Both the n values are highly correlated. For the floodplain, the flow resistance obtained from the velocity data also highly correlates with that obtained from 2D flow experiment.

RÉSUMÉ

Keywords: Flow resistance, floodplain roughness, bedforms, sediment transport rates, compound meandering channel, overbank flow.

1 Introduction

Conventional discharge prediction methods used in straight compound channels are not adequate when applied to a meandering channel due to the three-dimensional (3D) flow nature, and resulted in large errors in the estimation (Greenhill and Sellin, 1993). Greenhill and Sellin (1993) also reported a method of estimation of discharge in compound meandering channel using Manning's equation by extending the conventional division channel method. It was found that the method does not perform well in low relative depth, especially in wide main channel. Ervine and Ellis (1987) proposed a sub-sectional method based on energy loss within each subsection, to predict stage-discharge for compound meandering channel. Kiely (1990) reported that there is a tendency of this method to overpredict discharge at low flow relative depths and to underpredict discharge at high relative depths. Shiono *et al.* (1999) revisited the Ervine and Ellis's method, to investigate the energy loss due to secondary flow and turbulence in meandering channels with overbank flows using turbulence data obtained using a Laser Doppler Anemometer system. The results support the idea of using the horizontal plane division method at the shear layer interface between the main channel and floodplain. In addition to this, both the secondary currents and turbulence were found to make a significant contribution to

the total energy loss in the lower layer for shallow overbank flow. The energy losses due to contractions and expansions of flow were also found to be significant in high relative depth, but less in low relative depth. However, energy losses due to bed friction and shear at bankful level were found to be significant for shallow overbank flow.

As for flow resistance in compound channels, the extensive research on flow resistance in straight and meandering compound channels with mobile bed and fixed bed, rough and smooth floodplain was carried out in the Flood Channel Facility (FCF), located at HR Wallingford. In conjunction to this, the flow resistance in compound meandering channels has been subjected to recent investigations (Lyness *et al.*, 1998; Myers *et al.*, 1999, 2000; O'Sullivan, 1999). Myers *et al.* (1999) found that flow resistance in the meandering compound channels is significantly more complex than in a simple channel. The fixed bed main channel flow is greatly influenced by the floodplain roughness due to high momentum exchange between the main channel and floodplain flows. However, in mobile bed, the main channel resistance is independent of the floodplain roughness at low overbank flow. Lyness *et al.* (1998) and O'Sullivan (1999) investigated the effect of the main channel sinuosity to flow resistance, they concluded that the flow resistance in the main channel increases with the increases of sinuosity at low overbank depths, by a factor of approximately 1.5. Thus, flows in the main channel slow down at high sinuosity channels, which reduces discharge in the meandering channel.

As for sediment transport behaviour in compound meandering channels, O'Sullivan (1999) observed that sediment transport rate in the inbank flow increases with the flow depth and reaches a maximum at the bankful depth, and suddenly drops when the flow starts to inundate the floodplain. Ishigaki *et al.* (2000) and Shiono *et al.* (2001) reported a similar finding where a significant reduction in the sediment transport rate occurs in shallow overbank flow. They explained that such reduction is as a result of the increase in flow resistance that is induced by bedforms and momentum exchanges. This subsequently leads to the reduction in main channel velocity and boundary shear stress, hence the reduction of sediment transport rate.

There have been many studies on compound meandering channels in recent years. However the detailed variation in bed morphology along the meandering channel and the behaviour of sediment transport rates during floods with change in floodplain roughness have not been reported, in detail. The variation of flow resistance with water depth in meandering channel and floodplain with floodplain roughness is rarely seen in the literature. This paper provides some insight into such variation, to enhance our understanding of the physical processes involved in sediment transport mechanisms influenced by floodplain roughness within a compound meandering channel.

2 Experiments

The experimental set-up and method to measure velocity, bedforms and sediment transport rates in the compound meandering channel have been described, in detail, in Part I of this paper. This section describes two flume experiments to obtain basic flow parameters for compound channel flow analysis.

The first flume experiment was also conducted in a relatively small 4.0 m long and 0.3 m wide straight mobile channel with the same sand ($d_{50} = 0.885$ mm) to provide a formula of the sediment transport rate with the depth mean velocity and to establish flow resistance. The following experimental procedure was carried out to obtain data. After steady uniform flow condition was achieved through setting the same bed slope and water surface slope along the flume, the sediment transport rate was collected every 20 min for between 4 and 6 h continuously. During the experiment, the water depth and flow rate ranges were set to be between 20 and 30 mm and between 1.2 and 2.5 l/s, respectively. The Reynolds numbers were over 10,000. All the data were obtained with an aspect ratio greater than 10, which can be classified as a 2D flow condition.

The empirical formula, expressing a relationship between velocity and sediment transport rate, was obtained from the above experiment in the rectangular channel. In the literature, sediment transport rate normally relates to velocity squared (or bed shear stress), however a parabolic regression on the experimental data did not give a good fit, especially with the highest velocity data. When an exponential function was used, an improved fit was obtained. The optimum equation was

$$q_b = \left[6 \times 10^{-7*}\mathrm{Exp}(48.2 \times U_{\mathrm{d}})\right] - 0.02 \tag{1}$$

where q_b is the sediment transport rate per unit width and U_d is the depth-averaged velocity. This empirical formula is valid for the depth-averaged velocity up to 0.30 m/s, which is in our experimental range.

The sediment data with depth mean velocity are shown in Fig. 1 together with Eq. (1).

On the floodplain of the compound meandering channel, three types of roughness were used, i.e. smooth, artificial grass only and grass with blocks. The second flume experiments were conducted in a relatively larger 11 m long and 0.915 m wide flume with a bed slope of 0.002 to estimate the Manning n values for the grass and the grass with blocks,. The grass mats were laid on the sloping bed and the water depth changed from 20 to 86 mm to obtain a stage and discharge curve. All the data were again obtained under the condition of the aspect ratio greater than 10. From the stage–discharge curve, the Manning values were

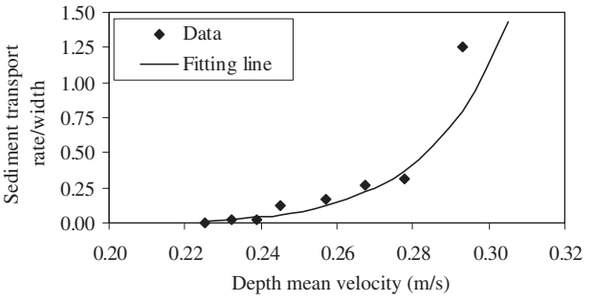

Figure 1 Sediment transport rate per unit width with depth mean velocity.

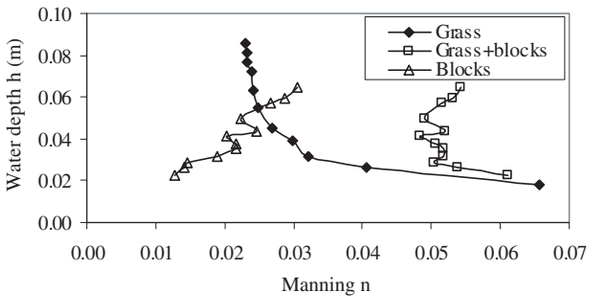

Figure 2 Manning coefficients with water depth for artificial grass, grass and blocks, and only blocks.

worked out with the Manning equation:

$$U = \frac{R^{2/3} S_0^{1/2}}{n} \tag{2}$$

where R is the hydraulic radius, U is the mean velocity, S_0 is the bed slope and n is the Manning coefficient.

Similarly, the stage–discharge curve for the grass with blocks was also obtained by placing the blocks on the grass mat, using the same arrangement of blocks used for the compound meandering channel experiment. The Manning coefficients of the grass mat with blocks could be then estimated. The total area of all the blocks on the channel is only 1% of the total channel area, hence the original channel width for the hydraulic radius was used. The Manning values for the grass, and grass with blocks are shown in Fig. 2. The Manning n values for blocks only were estimated by subtracting n values of the grass case, from n values of the grass with blocks case and are also shown in Fig. 2. As expected, Manning's n increases as water depth increases.

3 Beforms in the meandering channel for overbank flow

Bedforms were recorded by digital photogrammetry, and digital elevation model (DEM) were generated at 10 mm resolution using IMAGINE software (Chandler *et al*., 2001). To show distinctive features of bed form, the DEM images were represented in grey-scale image; darker colour indicating deeper parts of the channel, and lighter colour indicates shallower sections. Aerial views of the bedforms are shown in Figs 3–5 for G2, G5 and G7 cases, respectively, where water flows from left to right. For both G5 and G7 cases, the bedforms were fairly similar to that at the bankfull stage, in shallow overbank flow depths, therefore the bedforms were not measured.

Figure 3 shows a series of bed topographies created by flow regimes at the various water depths in the smooth floodplain G2 case. The bedform at the bankfull stage ($Dr = 0.0$) exhibits a typical bedform profile for inbank flow in a meandering channel as normally expected. Dr is the relative water depth defined by $(H-h)/H$, where H is the main channel water depth and h is the floodplain height. The deepest part appears near the outer bank, with a point sand bar formed from the inner bank of the apex section to the centre of the cross-over section.

At $Dr = 0.25$, the bedform starts to deviate from the typical bankfull pattern to a situation when irregular bedforms have

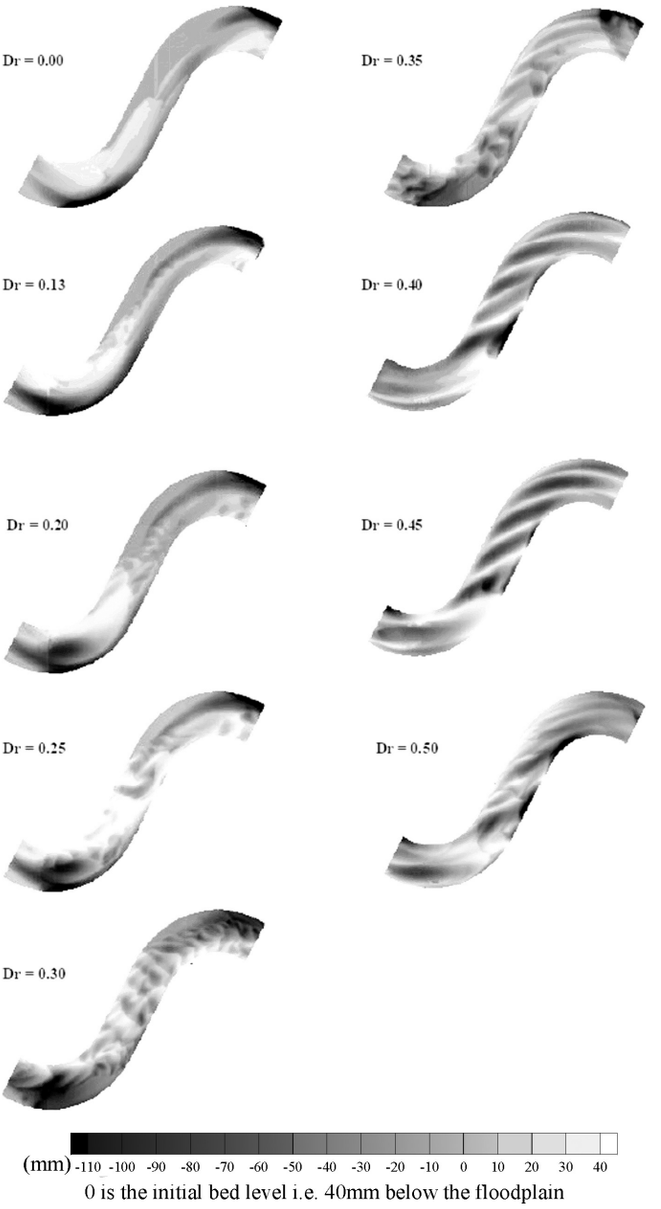

Figure 3 G2 bedforms for various overbank flows.

evolved. At $Dr = 0.30$, dunes and ripples were formed in the cross-over reach. They are irregular in shape with amplitudes between 10–30 mm. The dune and ripples disappears at depth ratio $Dr = 0.35$ and irregular sandbars start to form. At $Dr = 0.45$, very distinctive regular sand bars with a series of ridges are formed. The directions of the ridges are not in line with either the valley slope direction or the meandering channel direction. After $Dr = 0.50$, the wavy bedforms disappear and the channel bed becomes relatively planer. The diminishing of the bedforms inevitably reduces the effect of form friction on the overall friction in the channel.

In the G5 case, Fig. 4 shows two pools in the deeper regions located at the downstream apex from $Dr = 0.25$ to $Dr = 0.4$, whereas a shallower depth occurs in the inner region just after the bend (shown as the white colour). There is not much change in the bed topography up to $Dr = 0.40$. At $Dr = 0.45$, a number of ripples are formed at the downstream apex section. At $Dr = 0.55$,

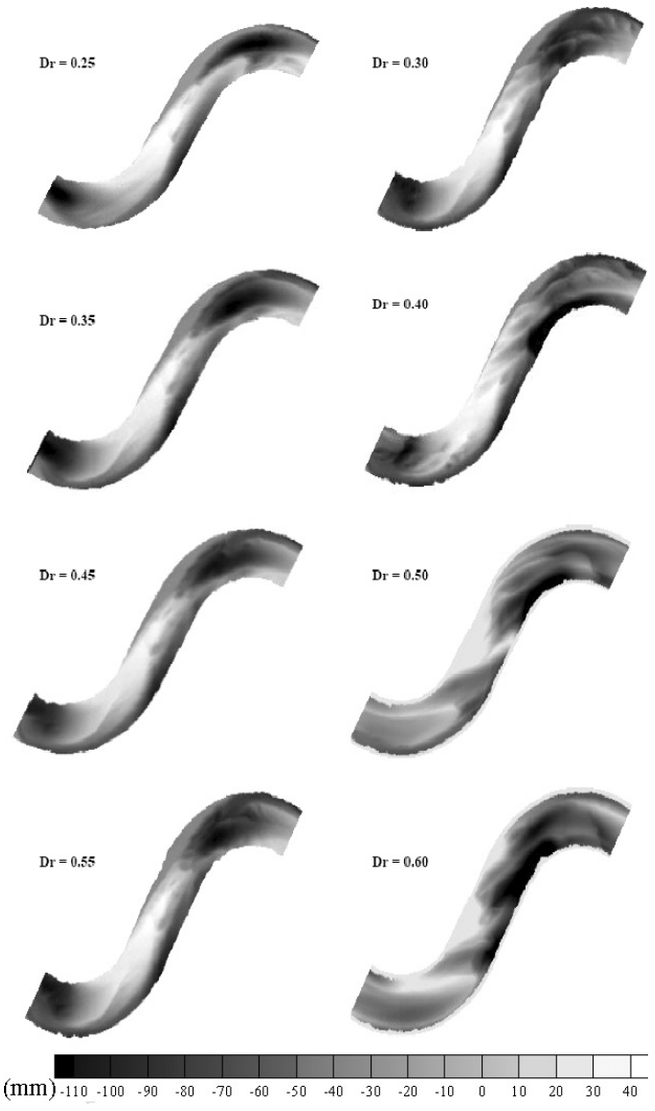

Figure 4 G5 bedforms for various overbank flows.

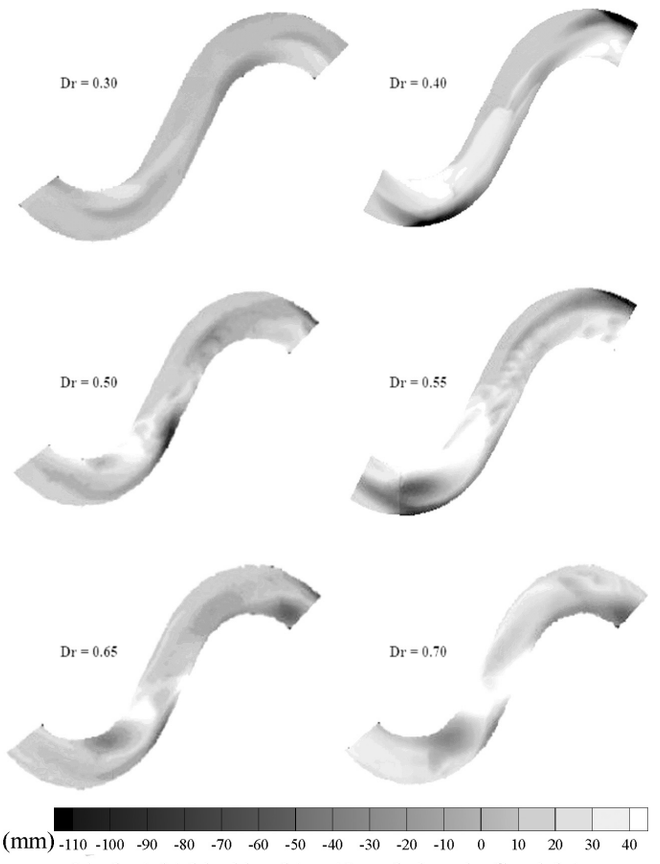

Figure 5 G7 bedforms for various overbank flows.

the ripples disappear, leaving a relatively large scouring region near the outer bank immediately after the cross-over section and regular ridges are formed. The regular ridges gradually disappear at $Dr = 0.60$.

In Fig. 5 for the G7 case, the bedform at $Dr = 0.30$ is fairly similar to that at the bankfull stage. The length of the sand bar is elongated at $Dr = 0.4$ but the fundamental shape of bedform remains the same up to $Dr = 0.50$. At $Dr = 0.55$, irregular bedforms consisting of dunes and ripples are seen along the cross-over section. At $Dr = 0.65$, the dunes and ripples disappear and at $Dr = 0.7$, relatively regular wavy bedforms appear in the bend region. It was observed during the experiment that sediment was transported from the main channel and deposited on the floodplain due to the strong "cross flow" at relatively high water depths for G2, G5 and G7 cases. The amount of sediment load migrating along the floodplain in the valley direction increased as the water depth increased. This deposited sediment moving along the floodplain contributes to an increase in floodplain flow resistance and causes a reduction in the channel depth as it re-enters the main channel (as indicated by the white area in the figure).

From the above figures for roughened floodplains, it is clearly seen that the bedforms significantly differ from those at the same relative depth in the smooth floodplain case (G2). The bed features in the roughened floodplain cases have much more irregular and variable patterns. However, as the floodplain roughness increases, the bedforms still tend to have similar characteristics, i.e. consisting of a point sand bar, ripples and dunes, wavy forms; returning to a plane bed as relative depth increases.

4 Sediment transport rates

Visualization of sediment movement was carried out using an underwater video camera, and confirmed that none of sediment was transported in suspension mode for any of cases examined. The sediment transport rate is therefore discussed in terms of bed load as this is the only transport mode observed during the experiments. Four mobile bed experiments in total were conducted to measure sediment transport rates, namely G1, G2, G5 and G7. Table 1 shows the configuration of compound channel.

For the purpose of rendering suitable data for comparison, each transport rate per unit width (q_b) was normalized by the transport rate per unit width (q_{bf}) at bankfull level. The normalised sediment transport rates with relative depths for four

Table 1 Configuration of compound channel

Total width (m)	Meander belt width (m)	Main channel width (m)	Cross-over length (m)	Side slope S_0	Radius of curvature (m)	Sinuosity	Valley slope
2.4	1.815	0.4	0.75	90^o	0.765	1.3837	1/500

Series name	Main channel aspect ratio	Bed mobility	Roughness element	Sediment size d_{50}(mm)
G1	5.33	Mobile	Smooth	0.855
G2	10	Mobile	Smooth	0.855
G5	10	Mobile	Grass	0.855
G7	10	Mobile	Grass+blocks	0.855

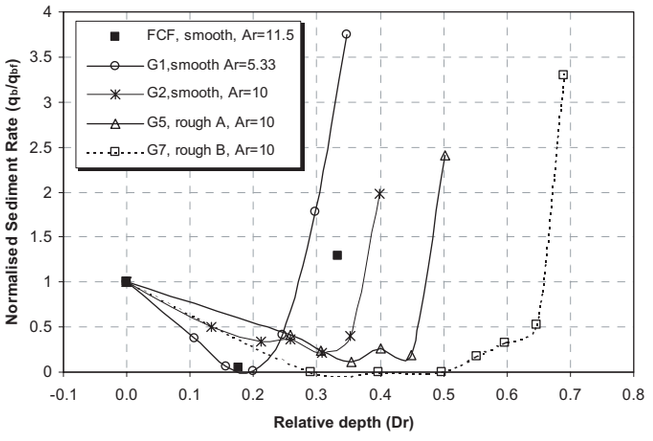

Figure 6 Normalized sediment rate relationships with various floodplain roughness.

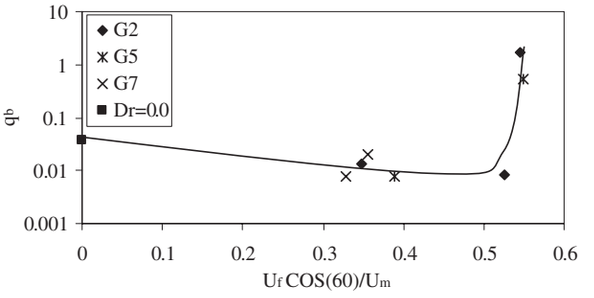

Figure 7 Sediment transport rate per unit width against the ratio of floodplain velocity component to main channel velocity.

experiments together with the data obtained from the Flood Channel Facility (FCF) at HR Wallingford are presented in Fig. 6. The FCF was 4 times the size of the Loughborough meandering compound channel, details of the FCF can be found in Rameshwaran *et al.* (1999). It can be seen from the figure that the sediment transport rate decreases until the relative water depth $Dr = 0.20$ for G1, $Dr = 0.35$ for G2, $Dr = 0.45$ for G5 and $Dr = 0.5$ for G7. This means that the depth to which sediment transport rate decreases, extends to a higher depth as the floodplain roughness increases. The reason for this is that as floodplain roughness increases, floodplain velocity reduces. As this reduced velocity enters the main channel a momentum exchange takes place between slower floodplain and faster main channel flows. As a result, the main channel velocity becomes slower over a wider range of water depths as the floodplain roughness increases.

Furthermore, the DEMs representing the bedforms illustrated in the previous section show a great variation of bedforms when water depth changes. From Figs 3–5, ripples and dunes distinctly appear in the cross-over section when the sediment transport rate is minimum. Wu and Wang (1999) reported that the resistance to flow due to this type of bed form could be more than 10 times that of the grain friction. Hence bedforms also play an important role in the reduction of the main channel velocity and sediment transport rate. This clearly indicates that floodplain roughness affects velocity, bed form and sediment transport rate in the main channel during flood.

From the flow structures presented in Part I of this paper, it is clear that the flow structure patterns for different roughened floodplains are more or less reproduced at different water depths. This indicates that the magnitude of floodplain flow controls the flow pattern and sediment transport rate in the main channel. The retardation and acceleration is caused by the shear generated by entering the floodplain flow into the main channel. The shear mainly occurs at the cross-over section and is generated by velocity difference between the main channel velocity and the main channel flow component of floodplain velocity (Shiono and Muto, 1998). Hence an investigation into the relationship between sediment transport rate and the magnitude of floodplain flow was undertaken. The floodplain velocity (U_f) was resolved into the component of the main channel flow direction, i.e. $\text{Cos}(60^0)*U_f$ in the cross-over section and was divided by the main channel velocity (U_m). The ratios $\text{Cos}(60^o)*U_f/U_m$ for G2, G5 and G7 were plotted against sediment transport rate per unit width in Fig. 7. In Case G1, velocities were not measured. The figure suggests that the sediment transport rate starts to increase above the ratio of approximately 0.5. Although this is a rough estimation from the figure, it can be said that the floodplain flow decelerates the main channel flow below the ratio of approximately 0.5, to reduce the sediment transport rate in this configuration of a meandering compound channel.

4.1 Flow resistance

There are many channel division methods, such as vertical, horizontal divisions and combined both, for discharge estimation in a two-stage meandering channel for overbank flow. For example, Ervine and Ellis (1987), Greenhill and Sellin (1993) and Shiono *et al.* (1999). However from the observed flow structures in Part I of this paper (Shiono *et al.*, 2007) and Shiono and Muto (1998), secondary flow circulations are situated in the upper and lower

Table 2 Flow parameters for G2, G5 and G7 using the measured velocity data

Case	H (m)	Dr	U_m (m/s)	n_m	Q (m^3/s)	Q_m (m^3/s)	Q_f (m^3/s)	U_f (m/s)	n_f
G2	0.0506	0.209	0.183	0.0245	0.0063	0.003607	0.002693	0.127	0.0170
G2	0.0581	0.312	0.175	0.0275	0.0111	0.004422	0.006678	0.184	0.0167
G2	0.0728	0.451	0.306	0.0176	0.0308	0.008937	0.021863	0.333	0.0138
G5	0.0727	0.450	0.201	0.0243	0.0157	0.004768	0.010932	0.156	0.0292
G5	0.0894	0.553	0.242	0.0251	0.0353	0.009074	0.026226	0.265	0.0227
G7	0.0893	0.450	0.182	0.0314	0.0178	0.006011	0.011789	0.120	0.0503
G7	0.1133	0.553	0.193	0.0352	0.0293	0.009248	0.020052	0.137	0.0572

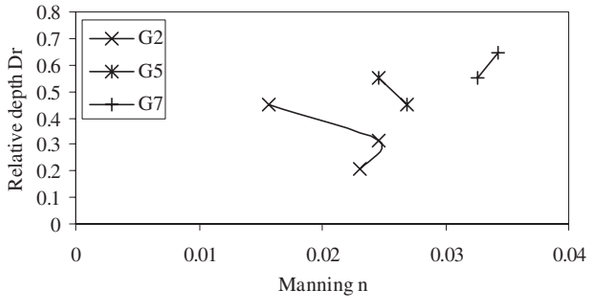

Figure 8 Manning n obtained from measured velocities with Dr in main channel.

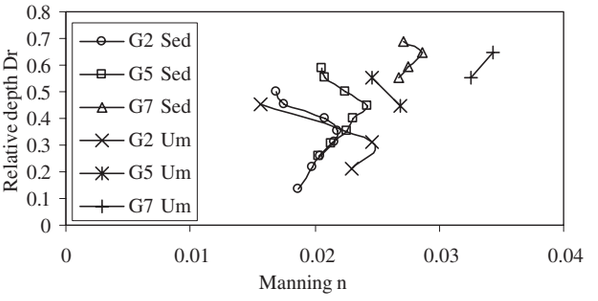

Figure 9 Manning n values obtained from sediment data and measured velocities with Dr in main channel.

layers in the main channel, therefore it is not appropriate to subdivide into two layers at the bankfull level using a horizontal plane to understand flow resistance during flood. In this study, the main channel is therefore considered as one sub section. The flow resistance used here is a Manning coefficient since it is popularly used by engineers. The Manning coefficients representing the main channel and floodplain were established using Eq. (2). S_o was the valley slope of 0.002 on the floodplain and the valley slope divided by a sinuosity of 1.38 in the main channel.

4.2 Flow resistance in the main channel

The discharge and mean velocity in the main channel were calculated from the measured velocities given in Part I of this paper (Shiono *et al.*, 2007). The mean velocities for G2, G5 and G7 were tabulated in Table 2. All n values for G2, G5 and G7 in the main channel were worked out using Eq. (2) and plotted in Fig. 8. It can be clearly seen from the figure that there is a maximum n value existing over water depth for G2, but it can not be seen for the other cases due to only two points for each case.

Since more sediment transport rate data are available, an attempt was made to calculate the Manning n using the sediment data for the roughened floodplain cases. To calculate the Manning n the mean velocity is required. The depth mean velocity was first worked out using Eq. (1) with the sediment transport rate data and then multiplied by the width of the channel as the initial bed profile (rectangular cross section) to estimate the mean velocity. The Manning coefficients were then estimated using Eq. (2). The estimated Manning coefficients from the sediment transport rates were plotted on Fig. 9, together with those obtained from the measured velocities, and this demonstrates that there is a maximum n value over water depth for each case. It is also noticed that most n values are smaller than those obtained from the measured velocities, except in the area of decreasing n for G2. This would be expected, since the velocity obtained from Eq.' (1) with the sediment transport data was assumed to be 2D flow. A mean velocity in 2D flow would be larger than that in 3D flow within a compound meandering channel. The higher the velocity, the lower the Manning n as can be seen from Eq. (2). As mentioned before, there is a maximum n value over water depth, which might have been expected from the minimum sediment transport rate observed over the water depth at which velocity should be minimum. The maximum n values increase 11% and 32% for G5 and G7, respectively, when compared with the maximum n for G2, therefore as the roughness on the floodplain increases the maximum flow resistance in the main channel also increases. With Fig. 7, the maximum flow resistance occurs at the ratio, U_f*Cos60^0/$U_{m,}$ of around 0.5.

To find the correlation between the Manning n values obtained from the measured velocity and the estimated velocity from the sediment data, both Manning n values at the same water depth, were plotted in Fig. 10. The best fit linear line achieved using 6 data points out of 7, has a gradient of 0.85 with a correlation coefficient of 0.85. It was judged that the erroneous point was an outlier from the other data. From the gradient of the best fit line the Manning n for the measured velocity case is roughly 15% larger than that for the sediment data case. This correlation gives a high degree of confidence to use the sediment transport rate data for understanding flow resistance behavior in the main channel.

4.3 Flow resistance on the floodplain

The Manning n values on the floodplain were obtained by two methods. The main channel discharge was first calculated using

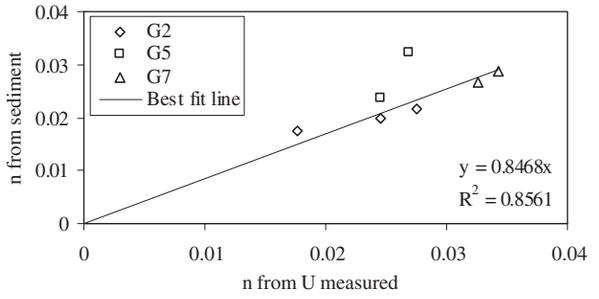

Figure 10 Correlation between Manning *n* values obtained from measured velocities and sediment data in main channel.

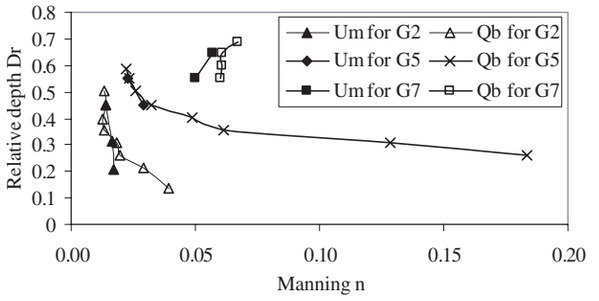

Figure 11 Manning *n* values obtained from sediment data and measured velocities with *Dr* on floodplain.

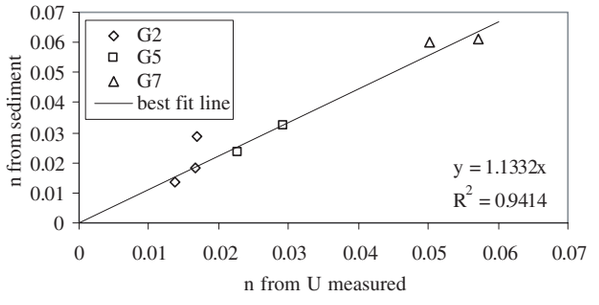

Figure 12 Correlation between Manning *n* values obtained from measured velocities and sediment data on floodplain.

both the measured velocities at the apex section and the estimated velocity from sediment transport data as described above. The floodplain discharge was then worked out by subtracting the main channel discharge from the measured total discharge. The mean velocity was finally estimated by the floodplain discharge divided by the floodplain area at the apex section, hence Manning *n* with Eq. (2).

For the floodplains, the *n* values obtained from the measured velocities and sediment transport rates are shown in Fig. 11. The Manning *n* values obtained from the measured velocities, follow the trend lines of the n values obtained from sediment data for all three different floodplain roughnesses. The correlation between them was also worked out (Fig. 12) together with the best fit line using 6 data points out of 7. From the gradient of the best fit line, the Manning *n* of the measured velocities is 13% smaller than that of the sediment transport rate case, which is a favourable direction, since it is 15% larger in the main channel.

An attempt was made to compare the n values of the measured velocities with the Manning *n* values of the grass only and grass

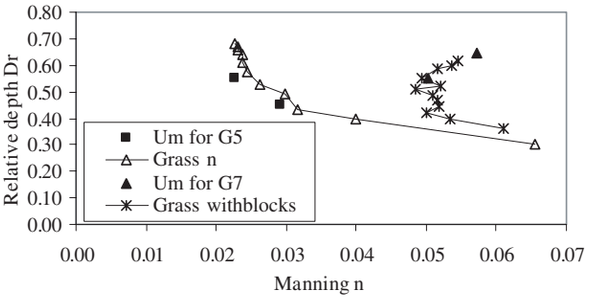

Figure 13 Manning *n* values obtained from sediment data and measured velocities with *Dr* on floodplain.

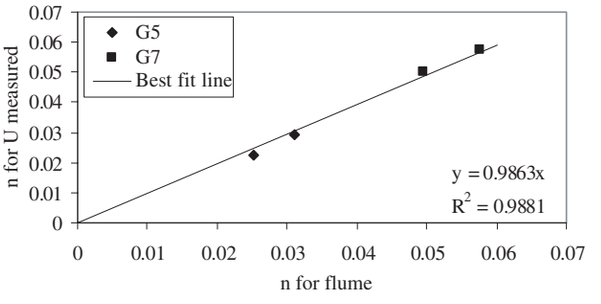

Figure 14 Correlation between Manning *n* values obtained from measured velocities and sediment data in main channel.

with blocks obtained during the flume experiment. Both Manning n values were plotted on Fig. 13. The Manning *n* values obtained from the measured velocities follow the trend lines of the *n* values of the flume experiment and the correlation between them was worked out and plotted (Fig. 14), together with the best fit line. The gradient of the best fit line is 0.986 almost 1.0, which means that the flow resistance on the floodplain is the same as the flow resistance studied in the flume experiments, i.e. the 2D flow condition in the relatively high water depth range ($Dr > 0.45$), despite 3D flow near the edge of main/floodplain along the meandering channel. This suggests that the effect of the 3D flow on the roughened floodplain flow is relatively small in this configuration whereas Shiono *et al.* (1999) reported that the energy losses due to contraction and expansion are significantly higher in the smooth floodplain case. In this study, the ratio of the total compound channel width to the main channel width was 6. As this ratio increases, floodplain flow becomes dominated for relatively high water depth, so the effect of the 3D flow on the floodplain flow is less and less significant, hence flow resistance on the floodplain tends to approach 2D flow floodplain roughness.

5 Conclusions

The bedforms, sediment transport rate and flow resistance in a meandering channel varying different floodplain roughness for overbank flow were investigated. Basic flow resistance and sediment transport data obtained from two relatively small flumes were used for the quantitative analysis of the flow resistance in the compound meandering channel. The following conclusions could be made.

The digital photogrammetry method to illustrate bedforms during flood gives, in detail, bedform variations along the meandering channel. DEM resolution of 10 mm were created, but higher resolutions could have been generated (3 mm). Such detailed representation of bedforms cannot be obtained using a point gauge. During overbank flow, the bedforms become irregular along the cross-over section at $Dr = 0.30$ for the smooth floodplain case and at higher water depths for the roughened floodplain cases. On the other hand, regular wavy bedforms were observed at $Dr = 0.45$ for the smooth floodplain case and also at higher water depths for the roughened floodplain cases.

The sediment transport rate first decreases to a certain water depth and then increases. The sediment transport rate is less than that of the bankfull case, until this depth, at which the ratio, U_f*Cos60^o/U_m is around 0.5. When this ratio becomes more than 0.5, the sediment transport rate starts to increase.

The Manning n in the main channel was calculated by two methods, using the measured velocities and sediment transport rates. A good Manning n correlation between two methods was obtained, which suggests that, with a high degree of confidence, the sediment transport rate data can be used to understand flow resistance behaviour if sediment transport rates are more accessible than velocity data. The maximum flow resistance occurs at the ratio, U_f*Cos60^o/U_m of around 0.5.

The Manning n values on the floodplain obtained from the measured velocities follow the trend lines of the n values of the 2D flume experiments and the correlation between them is nearly 1.0 for the roughened floodplain cases. This suggests that as floodplain increases roughness and water depth, flow resistance on the floodplain is approaching 2D flow floodplain flow resistance.

Acknowledgments

This research was conducted as part of the EPSRC project GR/L69213 and the authors would like to acknowledge the EPSRC for their financial support. The second author is grateful to the Overseas Research Studentship Award (OSR) and Department of Civil and Building Engineering, Loughborough University for providing the scholarship for his study.

Notation

B = Main channel width
Dr = Relative depth $(H - h)/H$
H = Main channel water depth
h = Water depth/ floodplain height
n = Manning coefficient
n_f = Floodplain Manning coefficient
n_m = Main channel Manning coefficient
Q = Total discharge
Q_f = Floodplain discharge
Q_m = Main channel discharge
q = Sediment transport rate
q_b = Sediment transport rate per unit width
q_{bf} = Bankfull sediment transport rate
R = Hydraulic radius
S_o = Bed slope
U = Mean velocity
U_d = Depth averaged velocity
U_f = Floodplain mean velocity
U_m = Main channel mean velocity

References

1. CHANDLER, J., SHIONO, K., RAMESHWAREN, P. and LANE, S.N. (2001). "Measuring Flume Surfaces for Hydraulics Research Using a Kodak DCS460". *Photogram. Record* 17(97), 39–61.
2. ERVINE, D.A. and ELLIS, J. (1987). "Experimental and Computational Aspects of Overbank Floodplain Flow". *Trans. Royal Soc. Edinbur. Earth Sci.* 78, 315–325.
3. GREENHILL, R.K. and SELLIN, R.H.J. (1993). "Development of a Simple Method to Predict Discharges in Compound Meandering Channels". *Proceedings of the Institution of Civil Engineers: Water, Maritime and Energy*, Vol. 101, pp. 37–44.
4. ISHIGAKI, T., SHIONO, K., RAMESHWARAN, P., SCOTT, C.F. and MUTO, Y. (2000). "Impact of Secondary Flow on Bed Form and Sediment Transport in Meandering Channels for Overbank Flow". *Annual Journal of Hydraulic Engineering*, Japan Society of Civil Engineers, Vol. 44, pp. 849–854.
5. KIELY, G. (1990). "Overbank Flow in Meandering Compound Channels — The Important Mechanisms". *International Conference on River Flood Hydraulics*. W.R. White, Chichester, England, John Wiley & Sons, pp. 207–217.
6. LYNESS, J.F., MYERS, W.R.C. and O'SULLIVAN, J.J. (1998). "Hydraulics Characteristic of Meandering Mobile Bed Compound Channels". *Proceedings of the Institution of Civil Engineers: Water, Maritime and Energy*, pp. 179–188.
7. MYERS, W.R.C., KNIGHT, D.W., LYNESS, J.F., CASSELLS, J.B. and BROWN, F. "(1999). "Resistance Coefficients for Inbank and Overbank Flows". *Proceedings of the Institution of Civil Engineers: Water, Maritime and Energy*, Vol. 136, pp. 105–115.
8. MYERS, R.C., LYNESS, J.F. and CASSELLS, J. (2000). "Influence of Boundary Roughness on Velocity and Discharge in Compound River Channels". *J. Hydraul. Res.* 39(3) 311–319.
9. O'SULLIVAN, J. (1999). "Influence of Planform and Boundary Roughness on Conveyance, Flow Resistance and Sediment Load Prediction in Meandering Channel". PhD Thesis, Ulster University, Ireland.
10. RAMESHWARAN, P., SPOONER, J., SHIONO, K. and CHANDLER, J.H. (1999). "Flow Mechanisms in Two-Stage Meandering Channel With Mobile Bed". *International Association for Hydraulic Research XXVIII Biennial Congress*, 22–27 August 1999, Graz, Austria, D6, p. 259.
11. SHIONO, K. and MUTO, Y. (1998). "Complex Flow Mechanisms in Compound Meandering Channel for Overbank Flow". *J. Fluid Mechan.* 376, 221–261.

12. SHIONO, K., MUTO, Y., KNIGHT, D.W. and HYDE, A.F.L. (1999). "Energy Losses Due to Secondary Flow and Turbulence in Meandering Channel with Overbank Flows". *J. Hydraul. Res. IAHR* 641–664.
13. SHIONO, K., RAMESHWARAN, P., CHAN, T., SPOONER, J. and CHANDLER, C.H. (2001). "Flow Mechanisms for the Reduction of Sediment Transport Rates in Meandering Channels at an Early Stage of Overbank Flow." *International Symposium on Environment Hydraulics*, Arizona, United States.
14. SHIONO, K., CHAN, T., SPOONER, J., RAMESHWARAN, P. and CHANDLER, C.H. (2007). "The Effect of Floodplain Roughness on Flow Structures, Bedforms and Sediment Transport Rates in Meandering Channels with Overbank Flows. Part (I)". *J. Hydraul. Res. IAHR*.
15. WU, W. and WANG, S.Y. (1999). "Movable Bed Roughness in Alluvial Rivers". *J. Hydraul. Eng. ASCE* 125(12) 1309–1312.